Accepted Manuscript

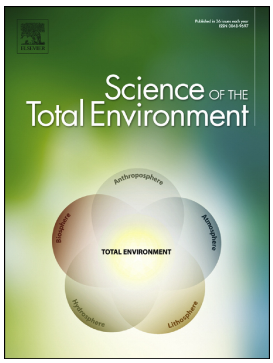

Mercury in tundra vegetation of Alaska: Spatial and temporal dynamics and stable isotope patterns

Christine L. Olson, Martin Jiskra, Jeroen E. Sonke, Daniel Obrist

PII: S0048-9697(19)30064-6
DOI: https://doi.org/10.1016/j.scitotenv.2019.01.058
Reference: STOTEN 30372

To appear in: *Science of the Total Environment*

Received date: 15 October 2018
Revised date: 5 January 2019
Accepted date: 6 January 2019

Please cite this article as: Christine L. Olson, Martin Jiskra, Jeroen E. Sonke, Daniel Obrist , Mercury in tundra vegetation of Alaska: Spatial and temporal dynamics and stable isotope patterns. Stoten (2019), https://doi.org/10.1016/j.scitotenv.2019.01.058

Mercury in tundra vegetation of Alaska: spatial and temporal dynamics and stable isotope patterns

Authors: Christine L. Olson[1], Martin Jiskra [2,3], Jeroen E. Sonke[2], and Daniel Obrist[1,4*]

Affiliations:

[1]Division of Atmospheric Sciences, Desert Research Institute, 2215 Raggio Parkway, Reno, Nevada 89512, USA.

[2]Geosciences Environnement Toulouse, CNRS/OMP/Université de Toulouse, 14 Avenue Edouard Belin, 31400 Toulouse, France.

[3]Environmental Geosciences, University of Basel, Bernoullistrasse 30, 4056 Basel, Switzerland

[4]Department of Environmental, Earth, and Atmospheric Sciences, University of Massachusetts, Lowell, MA, USA

*Corresponding author: Daniel Obrist (Daniel_Obrist@uml.edu), 978-934-3988

Abstract

Vegetation uptake of atmospheric mercury (Hg) is an important mechanism enhancing atmospheric Hg deposition via litterfall and senescence. We here report Hg concentration and pool sizes of different plant functional groups and plant species across nine tundra sites in northern Alaska. Significant spatial differences were observed in bulk vegetation Hg concentrations at Toolik Field station (52±9 μg kg^{-1}), Eight Mile Lake Observatory (40±0.2 μg kg^{-1}), and seven sites along a transect from Toolik Field station to the Arctic coast (36±9 μg kg^{-1}). Hg concentrations in non-vascular vegetation including feather and peat moss (58±6 μg kg^{-1} and 34±2 μg kg^{-1}, respectively) and brown and white lichen (41±2 μg kg^{-1} and 34±2 μg kg^{-1}, respectively), were three to six times those of vascular plant tissues (8±1 μg kg^{-1} in dwarf birch leaves and 9±1 μg kg^{-1} in tussock grass). A high representation of nonvascular vegetation in aboveground biomass resulted in substantial Hg mass contained in tundra aboveground vegetation (29 μg m^{-2}), which fell within the range of foliar Hg mass estimated for forests in the United States (15 to 45 μg m^{-2}) in spite of much shorter growing seasons.

Hg stable isotope signatures of different plant species showed that atmospheric Hg(0) was the dominant source of Hg to tundra vegetation. Mass-dependent isotope signatures (δ^{202}Hg) in vegetation relative to atmospheric Hg(0) showed pronounced shifts towards lower values, consistent with previously reported isotopic fractionation during foliar uptake of Hg(0). Mass-independent isotope signatures (Δ^{199}Hg) of lichen were more positive relative to atmospheric Hg(0), indicating either photochemical reduction of Hg(II) or contributions of inorganic Hg(II) from atmospheric deposition and/or dust. Δ^{199}Hg and Δ^{200}Hg values in vascular plant species were similar to atmospheric Hg(0) suggesting that overall photochemical reduction and

subsequent re-emission was relatively insignificant in these tundra ecosystems, in agreement with previous Hg(0) ecosystem flux measurements.

1 Introduction

Vegetation covers nearly 80% of the global terrestrial surface area (Schulze, 1982). Leaves greatly increase surface areas and thereby amplify exchanges of trace gases with the atmosphere up to seven times compared to barren ground surfaces (Asner et al., 2003). As such, vegetation provides an important terrestrial-atmosphere interface and is an important factor in the cycling and exchange of atmospheric pollutants with ecosystems, such as trace metals (Buch et al., 2015; Simonich and Hites, 1994), polycyclic aromatic hydrocarbons (Simonich and Hites, 1994), and traditional atmospheric pollutants such as ozone, NO_2, SO_2, and CO (Nowak et al., 2006). For mercury (Hg), a global pollutant with a long atmospheric residence time, vegetation plays a critical role in atmospheric deposition (Grigal, 2003; Jiskra et al., 2018; Obrist et al., 2011; Wang et al., 2016). At individual sites, particularly in forests, studies have long reported that atmospheric Hg uptake by aboveground plant tissues contributes significantly to atmospheric deposition (Lindberg, 1996; Munthe et al., 1995; Rea et al., 1996). This deposition occurs when plant shed leaves (litterfall) and other tissues or die (Grigal, 2003; Obrist et al., 2017; Obrist et al., 2011; Obrist et al., 2016; Schwesig and Matzner, 2001). Litterfall deposition of Hg typically exceeds Hg inputs by direct wet deposition (Wang et al., 2016; Grigal et al., 2000; Kolka et al., 1999; Rea et al., 2002). Globally, Wang et al. (2016) estimated a Hg deposition via litterfall of 1180 ±710 Mg yr^{-1}, which is over 20% of the total global atmospheric Hg burden. The vegetation uptake of atmospheric Hg and subsequent transfer to soils is large enough to drive seasonal patterns of atmospheric Hg concentrations on a global scale (vegetation Hg pump: Jiskra et al., (2018); Obrist et al., (2007)). Spatial analysis of Hg in soils show that soil Hg levels are strongly

linked to vegetation patterns, with lowest soil Hg concentrations found in barren locations (such as deserts) and highest soil Hg levels at sites with dense vegetation cover (Obrist et al., 2016). Similarly, soil Hg levels are strongly correlated with organic carbon concentrations across spatial scales (Obrist et al., 2011).

Hg stable isotope signatures are relatively new and powerful tools to assess sources and transformations of Hg in the environment. Atmospheric Hg(0) and Hg(II) in precipitation have distinct Hg isotope fingerprints, allowing differentiation of the two major atmospheric deposition pathways to terrestrial surfaces. Vegetation preferentially takes up lighter Hg(0) from the atmosphere leading to a characteristic mass dependent Hg isotope fractionation during vegetation uptake (Demers et al., 2013; Enrico et al., 2016; Yuan et al., 2018). Hg stable isotope studies across several ecosystems around the globe revealed that between 60 to 90 % of Hg in vegetation and soils originates from atmospheric Hg(0) deposited through vegetation uptake, rather than from Hg(II) in precipitation (Demers et al., 2013; Enrico et al., 2016; Jiskra et al., 2015; Wang et al., 2017; Zheng et al., 2016).

Many studies report that the source of Hg found in aboveground tissues of vegetation is dominantly derived from atmospheric Hg uptake (Ericksen and Gustin, 2004; Frescholtz et al., 2003; Grigal, 2003; Hanson et al., 1995; Millhollen et al., 2006; Rutter et al., 2011). Mechanisms of plant Hg uptake, however, are still unclear, but likely include both stomatal and nonstomatal pathways. Evidence for stomatal uptake can be inferred from i) controlled mesocosm studies with different soil and atmospheric Hg exposures (Frescholtz et al., 2003; Millhollen et al., 2006), ii) observations of diel fluctuations of gaseous elemental Hg(0) uptake along with CO_2 uptake (Millhollen et al., 2006; Obrist et al., 2008) and reductions of leaf Hg content when stomatal conductance is reduced (e.g., elevated CO_2; Millhollen et al., (2006)), iii) exposure

studies of leaves to spiked Hg isotopes (Rutter et al., 2011), and iv) by correlations of leaf Hg concentrations with the density of stomata (Laacouri et al., 2013). Non-stomatal uptake pathways can be inferred from dark deposition of Hg(0) (Stamenkovic et al., 2008).

Long-range atmospheric transport of Hg to the Arctic from the lower latitude is considered an important source of Hg to the Arctic (Dastoor et al., 2015; Dastoor and Larocque, 2004; Durnford et al., 2010; Steffen et al., 2015; Douglas and Sturm, 2004). In addition, the Arctic experiences enhanced deposition of atmospheric Hg(II) to snow and ice surfaces during bromine-induced conversion of Hg(0) to Hg(II) in the coastal atmosphere (termed Atmospheric Mercury Depletion Events [AMDEs]), which may provide additional deposition in the tens to hundreds of Mg to the Arctic each year (Ariya et al., 2004; Dastoor and Durnford, 2014; Lindberg et al., 2002; Skov et al., 2004). AMDEs occur during polar sunrise when a series of photochemical reactions rapidly oxidizes the dominant atmospheric Hg(0) to oxidized Hg(II) forms, which subsequently can deposit rapidly to Arctic snow and ice (Steffen et al., 2008; Moore et al., 2014). While Hg deposition from AMDEs can be a significant source, studies suggest that impacts are largely limited to near-coastal sites (Douglas and Sturm, 2004; Steffen et al., 2015; Van Dam et al., 2016) and that a substantial fraction of deposited Hg can re-emit to the atmosphere prior to snowmelt (Douglas et al., 2012; Ferrari et al., 2005; Johnson et al., 2008; Obrist et al., 2017).

To date, few studies report vegetation Hg dynamics in Arctic and subarctic environments, in particular also including bryophytes and lichens which are common plant functional groups in Arctic ecosystems (Campioli et al., 2009). In this study, we provide a detailed investigation of the role of vegetation in Arctic tundra Hg cycling. The study is part of a sequence of Hg studies from the northern Alaskan tundra recently providing information on terrestrial and soil Hg dynamics. Schuster et al. (2018) investigated permafrost Hg dynamics in northern soils and

showed that soils and permafrost layers contain an enormous amount (up to 1656 Mg) of Hg. Obrist et al. (2017) used a combination of stable Hg isotope analyses and direct flux measurements to show that Hg(0) deposition dominated (71%; 6.5 μg m^{-2} yr^{-1}) as a source of Hg in the interior Arctic tundra, rather than deposition via precipitation (~ 5%; 0.2 μg m^{-2} yr^{-1}) or by AMDEs (~24%; 2.5 μg m^{-2} yr^{-1}). They also indicated a dominant role of vegetation to drive Hg(0) deposition to the tundra, as shown by the strongest Hg(0) deposition rates after the spring onset of the tundra vegetation primary productivity. Olson et al. (2018) provided detailed data on active-layer tundra soil Hg concentrations and dynamics highlighting differences and sources in various soil horizons and showed that tundra soils, in particular B-horizons, contain large pools of Hg (184 Mg in the active layer). Agnan et al. (2018) examined Hg dynamics in wintertime snowpack across two winter seasons in the tundra providing evidence of consistently low concentrations of total and dissolved Hg and showing that photochemical reduction of Hg(II) to Hg(0) was largely absent at this site. In this study, we investigate vegetation Hg dynamics across multiple tundra sites and seasons in ten sites Arctic and subarctic Alaska, including a 200 km northern Alaska interior-to-coastal transect. We analyzed Hg vegetation concentrations in different plant functional groups and plant species in multiple tundra ecosystems; studied the temporal development of plant tissue Hg concentrations and spatial patterns using transect sites from inland areas to the Arctic coast; measured stable Hg isotope values in order to assess the origin and transformation of Hg within vegetation tissue; used analyses of key major and trace elements to further constrain sources and associations of Hg with other elements; calculated pools sizes and turnover (i.e., annual inputs) based on annual productivity and biomass inventories; and compared concentration and pools sizes of northern tundra vegetation with those reported in temperate locations.

2 Materials and Methods

2.1 Study Sites

Bulk vegetation samples and individual species were collected from nine study sites shown in **Figure 1**. The sites, which are described in detail in Olson et al. (2018), included: Toolik Field station in northern Alaska (68° 38' N, 149° 36' W); a transect of seven sites along a 200-km stretch of the Dalton Highway between Toolik Field station and Deadhorse near the Arctic Ocean; and a site located at Eight Mile Lake Observatory (EMLO) near the northeast corner of Denali National Park (63º 52' 42”N, 149º15' 12”W). The average tundra growing season in this region ranges from 50 days near the coast to 100 days near Toolik Field Station (Chapin and Shaver, 1996).

2.2 Sample collection

Vegetation Hg concentrations were determined from samples collected during the growing seasons of 2014, 2015, and 2016. Bulk vegetation samples were collected at all sites, and individual tundra species were collected as follows: at the main site at the Toolik Field station, we collected six different species including: C*arex aquatic* (tussock grass), *Betula Nana* (dwarf birch) leaves, *Masonhalea richardsonnii* (brown lichen), *Cetraria islandica* (white lichen) *Hylocomium splendens* (feather moss) and *Sphagnum* (peat moss). Four of the same species (tussock grass, dwarf birch, white lichen, and peat moss) were collected at EMLO. One of the species, tussock grass, was collected along with bulk vegetation along seven sites on northern transect along the Dalton Highway. Sampling always included four replicate samples at each site. For temporal patterns, samples were collected from four species (dwarf birch, tussock grass, white lichen, and feather moss) at the beginning and end of two growing seasons at Toolik Field

station to assess changes in plant Hg concentrations throughout the growing season. In addition to vegetation, organic surface soil horizons were sampled at each site (Olson et al., 2018). All samples were collected using clean latex gloves and were either hand-picked or cut using stainless steel scissors washed with deionized water, and samples were double-bagged in plastic zip-lock bags and stored on ice until transport to the laboratory where samples were kept frozen at -20˚C until analysis.

2.3 Sample preparation and analytical methods

Vegetation samples were oven-dried in a stainless steel drying oven (Lindberg Blue M Premium 3055, Thermo Fisher Scientific, Waltham, Massachusetts, USA) at 65℃ until weights of samples stabilized, generally after five days. Drying vegetation and soil temperatures at this temperature has shown not to result in Hg loss (Hojdová et al. 2015; Yang et al., 2017). Also note that samples were not washed prior to drying. After that, samples were ground using a stainless steel coffee mill. Samples were analyzed for Hg concentration using a total Hg analyzer (Model Nippon MA-2000, AGS Scientific Inc., Texas, USA) in accordance with U.S. EPA Method 7473 (EPA, 1998). The analyzer was calibrated using standard solutions (100 µg L^{-1} and 10 µg L^{-1}) prepared according to EPA Method 1631 (EPA, 2002). National Institute of Standards and Technology (NIST) solid standard reference materials (# 1575: Pine leaves: 39.9 µg Hg kg^{-1}; and # 1515: Apple Leaves: 44.4 µg Hg kg^{-1}) were measured at the beginning of each analytical run and repeated after every ten samples. When analysis of NIST standards deviated more than 5% from their values, the analyzer was recalibrated and samples run after the last acceptable NIST samples were re-run. All samples were analyzed in duplicates, and the arithmetic mean of duplicate values were reported. A total of 114 vegetation samples were analyzed for this study.

All samples from all sites also were analyzed for total carbon (TC) and total nitrogen (TN) at the Soil Forage and Water Analysis Laboratory at Oklahoma State University using a LECO dry combustion procedure (LECO, St. Joseph, MI). Other major and trace element concentrations in vegetation and soils from Toolik Field station included Mn, Cu, Zn, As, Br, Rb, Sr, Pb, Al, S, Cl, K, Ca, Cr, V, Y, Ti, Fe, Ni, and Si were measured by XRF analysis (Model Epsilon 5 Energy Dispersive X-Ray Spectometer, PANalytical, Netherlands). Using a resuspension technique (Chow et al., 1994), samples were loaded onto Teflon® filters. For filter analysis, EPA method IO 3.3 was used (U.S. EPA, 1999), and QA/QC procedures used are described in Chow et al., 1994. An energy-dispersive XRF miniprobe multi-element analyzer (EMMA, Cheburkin and Shotyk 1996) was used to measure major and trace elements in vegetation and soil samples collected along the Dalton Highway Transect sites. The EMMA analyzer was calibrated using certified reference materials.

2.4 Hg stable isotope analysis

We analyzed Hg stable isotope signatures using cold vapor multi-collector inductively coupled plasma mass spectrometry (MC-ICP-MS) as described previously (Enrico et al., 2016; Sun et al., 2013). In brief, dried and milled vegetation samples were combusted in a two-stage oven system and Hg was quantitatively recovered in an oxidizing acid trap (94 % ± 17 % recovery). Between 0.3 and 2 g (average 0.9 g) of plant material was processed and trap solutions were diluted to final concentrations of 0.5 and 1 ng/g, which corresponded to ^{202}Hg beam voltages of 0.2 and 0.4 V, respectively. Hg isotope ratios were measured using MC-ICP-MS (Thermo-Finnigan Neptune) at the Observatoire Midi-Pyrenees, France. Mass dependent fractionation (MDF) is expressed in delta notation (δ) relative to the bracketed NIST 3133 Hg standard:

$$\delta^{xxx}Hg = (^{xxx/198}Hg_{sample}/\ ^{xxx/198}Hg_{NIST3133} - 1)\ x10^3 \qquad (1)$$

where 'xxx' represents the mass of the measured Hg isotopes; 199, 200, 201, 202 and 204. Mass independent fractionation (MIF) is reported in capital delta (Δ) notation, representing the deviation of the measured delta values from the expected Mass dependent trend:

$$\Delta^{xxx}Hg = \delta^{xxx}Hg - \beta_{xxx} \times \delta^{202}Hg \quad (2)$$

where $\delta^{xxx}Hg$ represents the measured MDF value and β_{xxx} represents the kinetic mass-dependent scaling factors of 0.252 for ^{199}Hg, 0.502 for ^{200}Hg, 0.752 for ^{201}Hg and 1.493 for ^{204}Hg. The measurement uncertainty was assessed by repeated analysis of an in-house standard during the measurement sequences. The long-term reproducibility of the ETH-Fluka standard over the time period from 2016 to 2017 was $\delta^{202}Hg$, = 1.45±0.19‰, $\Delta^{199}Hg$ = 0.08±0.1‰, $\Delta^{200}Hg$ = 0.02±0.1‰, 0.03±0.1‰, -0.03±0.2‰ (2σ, n=73) which agreed with previously published values (Jiskra et al., 2015; Smith et al., 2015). To assess the performance of the overall sample pre-concentration and measurement procedure the standard reference material BCR-484, Lichen was repeatedly measured and results of $\delta^{202}Hg$, = 1.52±0.24‰, $\Delta^{199}Hg$ = -0.62±0.06‰, $\Delta^{200}Hg$ = 0.08±0.03‰, $\Delta^{201}Hg$ = -0.63±0.06‰, $\Delta^{204}Hg$ =-0.17±0.10‰ (2σ, n=5) agreed well with previously published values (Enrico et al., 2016; Estrade et al., 2010).

Using a mixing model, we calculated bulk vegetation Hg isotopic signatures using measured isotopic signatures of the different plant species collected at the site with their fraction of aboveground biomass (see 2.4) as follows:

$$\delta^{202}Hg(bulk) = f_1 * \delta^{202}Hg(f_1) + f_2 * \delta^{202}Hg(f_2) + f_3 * \delta^{202}Hg(f_3) + f_4 * \delta^{202}Hg(f_4)$$

$$\Delta^{200}Hg(bulk) = f_1 * \Delta^{200}Hg(f_1) + f_2 * \Delta^{200}Hg(f_2) + f_3 * \Delta^{200}Hg(f_3) + f_4 * \Delta^{200}Hg(f_4)$$

$$\Delta^{199}Hg(bulk) = f_1 * \Delta^{199}Hg(f_1) + f_2 * \Delta^{199}Hg(f_2) + f_3 * \Delta^{199}Hg(f_3) + f_4 * \Delta^{199}Hg(f_4)$$

where, f_1, f_2, f_3, and f_4 represent fractions of biomass for lichen, moss, grass, and dwarf birch.

2.5 Aboveground Biomass and Plant Hg Deposition

To estimate annual turnover of vegetation Hg and standing aboveground biomass pools, data on vegetation dynamics (aboveground net primary productivity: NPP; and aboveground vegetation biomass) were used from Shaver and Chapin (1991) and combined with measured tissue Hg concentrations. The percent abundance of common plant functional groups collected in this study was 43% for mosses, 23% for herbaceous leaves, 19 % for grasses, and 15% for lichen (Table S1). Annual aboveground plant Hg uptake was estimated using aboveground NPP estimates of lichen, bryophytes, graminoids, deciduous, and evergreen plants published in Shaver and Chapin (1991), which were multiplied with measured vegetation Hg concentrations for each respective functional group. Finally, we calculated standing aboveground vegetation Hg pool by multiplying the aboveground biomass by the respective Hg concentration. It is possible, that the percent abundance of plant functional groups and respective biomass could have shifted slightly since Shaver and Chapin's (1991) study.

3 Results and Discussions

3.1 Vegetation Hg Concentrations in Tundra Functional Groups

Hg concentrations of bulk vegetation and different plant species collected at Toolik Field Station in Alaska are shown in **Figure 2.** Mean vegetation Hg concentrations across all sites were as follows (from lowest to highest): dwarf birch leaves (8±1 μg kg^{-1}), tussock grass (9±1 μg kg^{-1}), white lichen (32±3 μg kg^{-1}), peat moss (34±2 μg kg^{-1}), brown lichen (41±2 μg kg^{-1}), and feather moss (58±6 μg kg^{-1}). Mean bulk vegetation measurements across the sites averaged 46±7 μg kg^{-1}. Overall, we observed lowest vegetation Hg concentrations in vascular plant tissues of annual

plants (i.e., tussock grass and dwarf birch leaves) and highest concentrations in nonvascular plants (i.e., lichen and mosses).

Differences in Hg concentration observed among collected plant species were relatively consistent across the multiple sites investigated. At Toolik Field Station, Hg concentrations of the nonvascular white lichen (39±3 μg kg^{-1}), brown lichen (43±1 μg kg^{-1}), and feather moss (63±3 μg kg^{-1}) were three to six times higher than those of vascular plant tissues (i.e., dwarf birch leaves: 13±0.4 μg kg^{-1}; tussock grass: 12±1 μg kg^{-1}). At the EMLO, Hg concentrations were 5-19 times higher in the nonvascular peat moss (38±2 μg kg^{-1}) and white lichen (25±1 μg kg^{-1}) compared to dwarf birch leaves (5±0.1 μg kg^{-1}) and tussock grass (2±0.4 μg kg^{-1}). Such differences were also observed across the Dalton Highway Transect with about four times higher Hg concentrations in peat moss (37±2 μg kg^{-1}) compared to tussock grass (10±1 μg kg^{-1}).

Higher Hg levels in mosses and lichen compared to vascular plants are commonly observed in northern areas and have been reported in the literature, and perennial plants generally show higher Hg concentrations compared to annual plants (Rasmussen et al., 1991; Hall and Louis 2004; Obrist et al., 2012). Hall and St. Louis, (2004) observed higher Hg concentrations in mosses (53-94 μg kg^{-1}) and in lichen (33 μg kg^{-1}), compared to birch leaves (7 μg kg^{-1}), pine needles (14 μg kg^{-1}), and herbaceous and shrub plants (6-27μg kg^{-1}) in northwestern Ontario. Analysis of over 400 vegetation samples in southern Ontario, Canada showed significantly lower Hg concentrations in vascular tree needles tissues (7-14 μg kg^{-1}) compared to nonvascular plants including mosses (30-75 μg kg^{-1}), lichen (37 μg kg^{-1}), and fungi (144 μg kg^{-1}) (Rasmussen et al., 1991). Landers et al., (1995) reported lichen and moss Hg concentrations from 20 to 112 μg kg^{1} and Hg concentrations in feather moss of 55 μg kg^{-1} across northern Alaska sites. Samples of *Racomitrium lanuginosum* (woolly fringemoss) and *Cetraria nivalis* (lichen) from Svalbard both

showed total Hg concentration of 113 µg kg^{-1} (Drbal et al., 1992). More recent measurements of Hg concentrations in moss and lichen across tundra sites in Greenland found Hg levels ranging from 30 to 540 µg kg^{-1} (Wojtun et al., 2013). In summary, these studies report overall similar patterns of concentrations across functional groups in northern ecosystems, with vascular plant concentrations roughly in the range of 5 to 25 µg kg^{-1}, moss concentrations in the range of 30 to 80 µg kg^{-1}, and lichen concentrations in the range of 30 to 120 µg kg^{-1}.

In **Figure 3**, we summarized Hg concentrations using Kernel density plots of Arctic vegetation Hg concentration from this study and six additional published Arctic studies with a total of 150 samples, separated by different functional groups including grasses, leaves, mosses, and lichen. Our best estimate of concentrations for lichen (n=46) ranged from 23–186 µg kg^{-1} with a mean and standard deviation of 64±6 µg kg^{-1}. Moss Hg concentrations (n=40) were similar, ranging from 19–195 µg kg^{-1} with a mean and standard deviation of 59±6 µg kg^{-1}.

Non-vascular plants such as lichen and mosses lack a vascular and developed root system; therefore, they accumulate water, nutrients, and metals from the atmosphere alone (Rühling et al., 1987; Shahid et al., 2017). Additionally, their large surface area allows substantial accumulation of heavy metals from the atmosphere (Shahid et al., 2017). Non-vascular plants can live for decades, thus prolonged exposure may lead to a high accumulation of metals (Holt and Bench, 2008; Riis et al., 2014; Willkomm et al., 1992). Lichen and mosses have been used as bioindicators of atmospheric trace metals (Rühling et al., 1987; Steinnes, 1995); for example, heavy metal concentrations in the lichen thalli are known to correlate with their atmospheric levels (Bari et al., 2001; Sloof, 1995). However, the application of lichen and mosses as passive monitors for Hg is limited (Berg and Steinnes, 1997; Dunec, 2008; Ikingura and Akagi, 2002; Nickel et al., 2015), possibly due to the fact that substantial fraction of Hg uptake occurs in

gaseous form and that different exposures to solar radiation causes different levels of photochemical re-emissions after deposition. Vascular plant uptake mechanisms include stomatal and non-stomatal uptake as well as possible xylem and phloem transport (Shahid et al., 2017). Yet, it has been conclusively shown that Hg in aboveground biomass in vascular plants also originates largely from atmospheric Hg uptake with little root contributions. Stable Hg isotope studies clarified that atmospheric Hg(0) accounts for the majority of Hg found in foliage (Demers et al., 2013; Enrico et al., 2016; Jiskra et al., 2015; Obrist et al., 2017; Zheng et al., 2016, see also section below). Vascular plants analyzed at our sites (tussock grass, dwarf birch leaves) are annuals that incorporate atmospheric Hg into their tissues for only one growing season before senescence, possibly further explaining their relatively lower tissue Hg concentrations compared to non-vascular tissues.

Wang et al. 2016 summarized vegetation Hg concentrations across 168 sites globally and estimated a mean vegetation Hg concentration of 54±22 μg kg^{-1}. Hence, the mean bulk vegetation Hg concentrations across all Alaska tundra sites (46±7 μg kg^{-1}) was similar to Wang et al.'s estimate of forest foliage in North America (43±12 μg kg^{-1}). Our data provides evidence that vascular vegetation Hg concentrations in the Arctic tundra is similar to that in forested areas across temperate sites, in spite of exposure to remote atmospheric Hg levels and substantially shorter growing seasons.

3.2 Spatial variability of Hg in vegetation and across central and northern Alaska

Spatially, bulk vegetation Hg concentrations were highest at Toolik Field station with a mean of 52±9 μg kg^{-1}, lower at EMLO (40±0.2 μg kg^{-1}) and lowest across the seven northern transect sites north of Toolik Field Station (30±5 μg kg^{-1}). Spatial differences in bulk vegetation Hg concentrations may be attributable to different representation of species or functional groups; for

example, moist nonacidic tundra and moist acidic tundra are more common closer to the Brooks Range and wet sedge tundra are more common closer to the coast (Muller et al., 1999). However, decreases in Hg concentrations also were observed for the species that were collected across multiple transect sites. For example, compared to Toolik Field station, Denali species showed Hg concentrations that were 49% lower in dwarf birch, 19% lower in tussock grass, 33% lower in white lichen, but in contrast 50% higher in peat moss. A paired t-test showed these decreases between sites to be statistically significant (tussock grass, white lichen, and peat moss: $P < 0.05$; dwarf birch: significant only the 10% confidence level, $P = 0.07$). Generally, higher vegetation Hg concentrations at Toolik Field station (with the exception of peat moss) was in contrast to our expectations of lower plant Hg concentrations in the more remote northern tundra being farther from anthropogenic pollution sources (Jaeglé et al., 2010).

Across the 200 km northern tundra transect, vegetation Hg concentrations showed substantial concentration variability. Mean bulk vegetation Hg concentrations significantly decreased with latitude by 24% (paired t-test: $P < 0.01$, **Fig. 4**), and highest bulk vegetation Hg concentrations were observed near the Brooks Range and Sagwon Hills area and lowest at sites nearer to the coast. The patterns contrasted our expectations that vegetation Hg concentrations would increase towards the Arctic coast due to potential impacts of AMDEs. This is consistent with minor impacts of AMDEs observed at Toolik Field station using direct deposition measurements and stable Hg isotope data (Obrist et al., 2017). It is further consistent with minor impacts of AMDEs observed in snowpack Hg levels in interior snowpack: for example, Douglas et al. (2004) observed a sharp decrease in snow Hg concentrations less than 30 km from the Alaskan Arctic coast, and Agnan et al. (2018) measured no enrichment of snowpack Hg concentration at surface layers of snow across the same northern transect from Toolik Field station to the Arctic coast.

Reasons for decreased Hg concentrations in bulk vegetation with increasing latitude may include a shorter growing season in northern sites (e.g., snowmelt has been estimated about nine days later in the coastal plains compared to the foothills near the Brooks Range (Narasimhan and Stow, 2010) or differences in plant productivity and plant species composition across sites.

Other studies reported different coastal-to inland gradients of Hg loadings: for example, along the northern Norwegian coast, significant gradients in vegetation Hg concentrations were observed and attributed to different atmospheric Hg deposition, with substantially higher total Hg in moss collected along the coast compared to those collected further inland (Steinnes et al., 2003; Steinnes and Sjobakk, 2005). Bargagli et al. (2005) and Carignan and Sonke, (2010) reported elevated Hg concentrations in coastal lichen and mosses compared to inland sites. Although Hg levels in tundra vegetation did not increase towards the coast in our study, we observed that coastal proximity led to increases of other trace elements associated with coastal sources. XRF spectroscopy analysis of vegetation samples showed 2-10 times enrichment of K, Sr, S, Br, S, Cl, and Zn at the transect site closest to the ocean, and many of these elements are commonly associated with coastal and oceanic sources (Derry and Chadwick, 2007; Nakano et al., 2012; Reimann et al., 2009). Additionally, some of these elements are susceptible to transportation during weathering processes because of their high solubility (Carling et al., 2017; Santolaria et al., 2017).

Our data also provide evidence that dust may have contributed to spatial differences. At sites where vegetation was high in Hg along our transect (**Fig. 4**, sites 1, 4, and 5)**,** we correspondingly observed higher abundances of elements associated with dust (**Fig. S1**; i.e., Fe, Ti, V, and Ni; (McTainsh and Strong, 2007; Santelmann and Gorham, 1988)). Using linear regression analysis, we observed statistically significant positive correlations of these trace

elements with Hg, in particular for V (r^2=0.86; P<0.01) and Ti (r^2=0.85; P<0.01), and also for Si (r^2=0.52; P<0.01), Ni (r^2=0.34; P=0.01), Y (r^2=0.53; P<0.01), and Fe (r^2=0.47; P<0.01). When assessing spatial gradients of V and Ti, these elements showed close similarities with the distribution of Hg following the same order of concentrations across sites (**Fig. S1**). We propose that wind remobilization of loess from soils and glacial deposits may redistribute dust elements, including Hg, across the Arctic coastal plain. Vegetation sampling was performed at the end of the growing season in August when surface tundra soils were driest. In addition, the transect sites were located within several hundred meters to one kilometer from the Dalton Highway, a commercial route for transport to the Prudhoe Bay oil fields whereby truck traffic may have mobilized dust. Dust inputs have been shown to be an enrichment sources of trace and heavy metals to vegetation (Brumbaugh et al., 2011; Ram et al., 2014; Shotyk et al., 2016). For instance, in Shotyk, et al. (2016) heavy metals within peat moss in bogs of northern Alberta were highly correlated with dust inputs from the nearby Athabasca Bituminous Sands region.

3.3 Evolution of Vegetation Hg Concentration over the Growing Season

Early and late season sampling of tundra vegetation in 2015 and 2016 showed substantial increases in Hg in foliar tissues within the short tundra growing season, which rarely lasts more than 100 days (Chapin and Shaver, 1996). Between June/July sampling versus August/September sampling, dwarf birch leaves, tussock grass, white lichen, and feather moss all showed increases in plant Hg concentrations, ranging from +1 μg kg^{-1} in tussock grass to +23 μg kg^{-1} in white lichen (**Fig. 5**). Dwarf birch showed the highest increase in Hg concentrations (+61%) followed by white lichen (+43%), feather moss (+26%), and tussock grass (+11%). Paired t-test showed these seasonal increases to be statistically significant for dwarf birch, white lichen, and feather moss (all P<0.01), but not for tussock grass (P = 0.41). The rate of Hg

concentration increase was 0.12 μg kg^{-1} day^{-1} for dwarf birch, 0.38 μg kg^{-1} day^{-1} for white lichen, and 0.23 μg kg^{-1} day^{-1} for feather moss. Increases in Hg concentrations in plant foliage during the growing season has been observed in many temperate studies, including in grasses (Millhollen et al., 2006; Rea et al., 2002) and tree species (Ericksen et al., 2003; Rasmussen, 1995; Rea et al., 2002). For example, concentrations of Hg in forest foliage increased 10-fold from springtime bud break to autumn litterfall (corresponding to approximately 0.29 μg kg^{-1} day^{-1}) in deciduous trees in Vermont and Michigan (Rea et al., 2002). Rasmussen (1995) observed that Hg concentrations more than doubled in pine needles of balsam fir (*Abies balsamea*) and in white spruce (*Picea glauca*) across a 160-day growing season, with daily Hg enhancement of approximately 0.1 μg kg^{-1} day^{-1} in spruce needles and 0.07 μg kg^{-1} day^{-1} in fir needles. Our observed Hg increases in tundra vegetation ranging from 0.12-0.38 μg kg^{-1} day^{-1} thus fell within the similar range observed in temperate forests sites (0.07-0.29 ng g^{-1} day^{-1}).

3.4. Hg Stable Isotopes in Tundra Vegetation

Mass-dependent (δ^{202}Hg, MDF) and mass-independent (Δ^{199}Hg, MIF) signatures are widely used to constrain Hg sources, fate, and bioaccumulation (Bergquist and Blum, 2009; Blum et al., 2014; Obrist et al., 2017; Sonke, 2011; Yin et al., 2016; Yin et al., 2014). Hg stable isotopes allow for differentiation between foliar uptake of atmospheric Hg(0) and Hg(II) wet deposition and thus provide important information on the deposition pathway (Demers et al., 2013; Enrico et al., 2016; Jiskra et al., 2015). Reduction of Hg(II) to Hg(0) can lead to a revolatilization of Hg which is associated with characteristic stable isotope fractionation trajectories (Bergquist and Blum, 2007; Kritee et al., 2007; Blum et al., 2010; Zheng and Hintelmann, 2010a; Zheng and Hintelmann, 2010b; Jiskra et al., 2015; Yuan et al., 2018).

We measured δ^{202}Hg, Δ^{199}Hg and Δ^{200}Hg of different plant species collected at the Toolik Field Station, which included feather moss, brown lichen, white lichen, tussock grass, and dwarf birch leaves to investigate the source of Hg deposition and re-emission processes. Hg isotope signatures of individual plant species are compared to bulk vegetation, Hg(II) in wet deposition and atmospheric Hg(0) previously reported for the same site in Obrist et al., (2017). Based on an endmember mixing model using triple isotopic signatures, Obrist et al., (2017) showed that approximately 90% of Hg in bulk vegetation at Toolik Field station was derived from atmospheric Hg(0). Overall, δ^{202}Hg, Δ^{199}Hg and Δ^{200}Hg values for all vegetation samples ranged from -1.95 to -0.52 ‰, -0.41 to 0.71 ‰, and -0.07 to 0.16 ‰ respectively (**Fig. 6**).

In regards to MDF, mean δ^{202}Hg values followed the order (from heaviest to lightest): brown lichen (-0.72±0.06 ‰) > white lichen (-0.89±0.08 ‰) > tussock grass (-1.29±0.13 ‰) > dwarf birch leaves (-1.39±0.13 ‰) > feathermoss (-1.42±0.07 ‰) > bulk vegetation (-1.43±0.08 ‰). Such differences in δ^{202}Hg values of species relative to atmospheric Hg(0) may be explained by different uptake mechanisms which are associated with different fractionation factors (i.e., stomatal, nonstomatal, or by diffusion (Koster van Groos et al., 2014; Stamenkovic and Gustin, 2009); or alternatively by different contributions of atmospheric Hg(II) (see discussion below). Uptake of atmospheric Hg(0) into vascular plants results in large shifts in δ^{202}Hg values because plants preferentially take up light Hg isotopes (Demers et al., 2013; Enrico et al., 2016; Sun et al., 2017; Yin et al., 2013; Yuan et al., 2018). Demers et al. (2013) observed that foliar uptake of atmospheric Hg by aspen foliage induced a large (-2.89 ‰) shift in δ^{202}Hg values compared to Hg(0). More recently, Sun et al. (2017) measured δ^{202}Hg ranging from -2.67 to -0.87 ‰ in tissues of mangrove plants collected in China. Enrico et al. (2016) derived a fractionation factors of -2.6 ‰ for δ^{202}Hg between atmospheric Hg(0) and sphagnum, pine needles, *calluna* leaves

and lichen at a Pinet bog in the French Pyrenees. In our study, δ^{202}Hg values of vegetation relative to atmospheric Hg(0) showed shifts of -2.09 ‰ in feather moss, -2.06 ‰ in white lichen, -1.96 ‰ in dwarf birch, -1.56 ‰ in tussock grass, and -1.39 ‰ in brown lichen. However, simple determination of enrichment factors relative to atmospheric Hg(0) does not account for possible contributions of Hg(II) deposition or isotopic fractionation during post deposition processes.

In regards to MIF, mean Δ^{199}Hg values overall were positive in brown lichen (0.23±0.02 ‰) and white lichen (0.17±0.11 ‰), whereas all other samples exhibited negative Δ^{199}Hg values (e.g. feathermoss: -0.11±0.02 ‰; tussock grass: -0.06±0.04 ‰; and dwarf birch leaves: -0.28±0.03 ‰). Bulk vegetation also showed negative Δ^{199}Hg values (-0.2±0.01 ‰). In comparison, atmospheric Hg(0) measured at Toolik Field station showed Δ^{199}Hg values of -0.25±0.07 (n=6; Obrist et al, (2017)), so that all but dwarf birch leaves were statistically different from the atmospheric Hg(0) signature. Negative shifts in Δ^{199}Hg values relative to atmospheric Hg(0) (by -0.1 to -0.3 ‰) have been previously reported for vascular plants (trembling aspen, paper birch, sugar maple, sphagnum, e.g., Demers et al., (2013), Zheng and Hintelmann, (2010a), Enrico et al., (2017)); these shifts are attributed to photoreduction and re-emission of foliar Hg(II) in analogy to laboratory experiments that showed depletions of odd-mass isotopes in residual fractions during photochemical reduction of Hg(II) complexed to reduced sulfur thiol groups (Zheng and Hintelmann, 2010a). This interpretation has recently been constrained by flux bag experiments showing that re-emitted Hg(0) was associated with positive Δ^{199}Hg anomalies relative to Hg in foliage (Yuan et al., 2018). Hence, Δ^{199}Hg values of dwarf birch leaves sampled at Toolik Field station, which lacked significant shifts of Δ^{199}Hg compared to the atmospheric Hg(0) signature, suggest that radiation under the Arctic conditions may not be strong enough to

cause significant d in dwarf birch leaves. This would be consistent with a generic absence of re-emissions of Hg(0) in direct micrometeorological flux measurements at this site, including in summer months (Obrist et al., 2017).

In contrast, we observe positive Δ^{199}Hg in brown and white lichen from Toolik Field station and a positive correlation between Δ^{199}Hg and δ^{202}Hg for all data. Most reported data on lichen show Δ^{199}Hg values depleted in odd isotopes relative to atmospheric Hg(0) (-0.41±0.28, n=83; Carignan et al., 2009; Demers et al., 2013). The reported shift in Δ^{199}Hg in lichen towards more negative values is analogue to observations from vascular plants (Demers et al., 2013; Enrico et al., 2016) and has been explained by photochemical reduction of Hg(II) bound to thiol groups (Zheng and Hintelmann, 2010a). Blum et al. (2013), however, also reported shifts in Δ^{199}Hg values towards more positive values relative to atmospheric Hg(0) in lichen collected close to a mining and energy production site, possibly attributable to photochemical reduction of Hg(II) complexed by non-thiol compounds (Bergquist and Blum, 2007; Zheng and Hintelmann, 2009; Zheng and Hintelmann, 2010a). Therefore, positive Δ^{199}Hg values in brown and white lichen from Toolik Field station could be explained in two ways: i) photochemically driven re-emission of non-thiol bound Hg (Zheng and Hintelmann, 2010a), or ii) binary mixing between Hg(0) uptake by foliage and atmospheric Hg(II) deposition (both wet and dry) (Enrico et al., 2016, 2017). Our limited Hg(II) wet deposition data (n=3) at Toolik supports the binary mixing hypothesis, but isotope observations on Hg(II) dry deposition are lacking. Hg input from dust deposition is expected to have no significant Δ^{199}Hg and Δ^{200}Hg anomalies similar to geogenic Hg measured in rocks at the same site (Obrist et al., 2017). A significant contribution of Hg from dust as suggested by other trace metals is plausible from the observed Hg stable isotope

variability in the plants, however it cannot explain positive Δ^{199}Hg and Δ^{200}Hg values observed in brown and white lichen.

To date, it is thought that Δ^{200}Hg signatures are insensitive to photochemical modification in the Earth's critical zone (Enrico et al., 2016). Δ^{200}Hg can therefore potentially be used to further explore the above two hypotheses. **Figure 6** shows δ^{202}Hg vs. Δ^{200}Hg in the Hg(II) wet deposition (n=3) and Hg(0) end-members and vegetation at Toolik. However, due to small Δ^{200}Hg variation relative to analytical uncertainty, and the limited number of end-member samples taken only during the dark winter, we cannot currently use Δ^{200}Hg to estimate Hg(II) and Hg(0) contributions to vegetation Hg.

3.5 Estimation of Aboveground Hg pools and Vegetation-Derived Deposition

To estimate the contribution of plant Hg deposition to tundra soils through senescence and litterfall decomposition, we combined data on annual tundra plant productivity and turnover rates (Shaver and Chapin, 1991) with measured plant Hg concentrations from the Toolik Field station. **Table S1** shows aboveground net primary productivity and standing biomass of common tundra vegetation types at the Toolik Field station, their respective Hg tissue concentration, and calculated aboveground biomass Hg pool. Substantial Hg mass was found to be contained in aboveground vegetation (29 μg m^{-2}) which can subsequently be transferred to tundra soils via plant senescence and litterfall. Notably, Hg mass estimated to reside in Arctic vegetation falls within the range of foliar Hg mass estimated for densely forested ecosystems of the western United States (15-45 μg m^{-2}; Obrist et al., 2016). Highest amounts of aboveground biomass were associated with mosses (35%) and woody tissues (24%), with lower contributions in graminoids (16%), deciduous type vegetation (13%), and lichen (12%) (**Table S1**). Mosses, in particular, showed both highest aboveground biomass and Hg concentrations, resulting in particularly high

aboveground vegetation Hg pool (16.5 µg m^{-2}), approximately four times that of lichen (3.8 µg m^{-2}) and six times that of graminoids (3.0 µg m^{-2}). The estimated aboveground biomass representation can be independently verified by stable isotope values of different functional plant groups. Using a mixing model of the different isotope values reported for different plant functional groups above, the calculated isotopic signatures for bulk vegetation agrees well with that of measured bulk vegetation (δ^{202}Hg (-1.31 ‰ vs. -1.43 ‰), Δ^{199}Hg (-0.21 ‰ vs. -0.20 ‰), and Δ^{200}Hg (0.00 ‰ vs. -0.02 ‰).

In Obrist et al., (2017) and in **Table S1** we provided estimates of total plant-derived Hg deposition via by litterfall of 8 µg m^{-2} yr^{-1} and noted that plant-derived deposition greatly exceeded deposition via wet deposition (0.2 µg m^{-2} yr^{-1}) and via AMDEs (2.5 µg m^{-2} yr^{-1}) at this site (Obrist et al., 2017). Our estimated plant-derived Hg deposition of 8 µg m^{-2} yr^{-1} was at the lower range compared to sites in the lower 48 U.S. states. For example, Risch et al. (2012) estimated a median Hg litterfall deposition rate of 12 µg m^{-2} yr^{-1} with a range of 4-23 µg m^{-2} yr^{-1} across forests in the eastern United States, and Risch and Kenski, (2018) measured litterfall deposition rates between 10-23 µg m^{-2} yr^{-1} with a median of 16 µg m^{-2} yr^{-1} across five states in the Midwestern US. To our knowledge, no study has estimated tundra plant Hg deposition rates before. The observed plant-derived Hg deposition associated with tundra vegetation is surprisingly high, in particular given the short growing season in this arctic tundra between 50 to 100 days (Chapin and Shaver, 1996). A critical reason for relatively high vegetation Hg deposition across the Arctic tundra likely are relatively high Hg concentrations in lichen and mosses and their importance for biomass productivity (e.g., jointly accounting for up to 49% of the standing aboveground vegetation; **Table S1**).

4 Conclusions

Arctic vegetation plays an important role for Hg dynamics in the arctic and subarctic tundra of Alaska. Despite the short growing season and remoteness from pollutant sources, measured vegetation Hg concentrations fell within the range of those reported in temperate sites, with Hg mass contained in aboveground tundra vegetation (29 μg m^{-2}) being similar to those reported for densely forested ecosystems of the United States. This considerable mass of Hg contained in tundra vegetation provides a significant pool available for subsequent deposition via litterfall and senescence. A reason for relatively high Hg pools in tundra aboveground biomass is a high representation of mosses and lichen (accounting for ~ half of total aboveground biomass) with inherently high Hg tissue concentrations. Significant spatial gradients exist across various tundra sites, with decreasing Hg vegetation concentrations from inland towards the Arctic Ocean, providing little evidence of enhanced Hg deposition due to AMDEs. Finally, multi-element characterization show that Hg in vegetation was correlated with typical crustal elements (e.g., Fe, Ti, V, and Ni) possibly indicating dust as a source of Hg concentration in vegetation.

Hg stable isotope signatures of different plant species constrained that atmospheric Hg(0) was the dominant source of Hg in vegetation. Mass-dependent isotope signatures (δ^{202}Hg) in vegetation relative to atmospheric Hg(0) showed pronounced shifts towards lower values consistent with previously reported isotopic fractionation during foliar uptake of Hg(0). Mass-independent isotope signatures (Δ^{199}Hg) of lichen were more positive relative to atmospheric Hg(0), indicating photochemical reduction of Hg(II) or higher contributions of inorganic Hg(II) from atmospheric deposition and/or dust. In general, however, Δ^{199}Hg and Δ^{200}Hg values in vascular plant species were similar to atmospheric Hg(0), suggesting that overall photochemical reduction and subsequent re-emission was relatively insignificant in these tundra ecosystems (Obrist et al., 2017).

Climate warming in the Arctic has led to an increase in the vegetation growing season of about one week over the last 30 years (Park et al., 2016). Climate change will continue to lead to shifts in the composition, density, and distribution of Arctic vegetation (Bjorkman et al., 2018; Pearson et al., 2013; Tape et al., 2006). For example, half of Arctic vegetated areas may experience a shift to a different physiognomic class such as an increase in woody cover (Pearson et al., 2013). Shrub cover has already increased in northern Alaska over the past 50 years, particularly on hill slopes and valley bottoms (Tape et al., 2006). Given strong species-specific differences in tissue Hg concentrations, such widespread shifts in Arctic vegetation is likely associated with changes in the deposition and cycling of Hg in tundra ecosystems.

References

Agnan Y, Douglas TA, Helmig D, Hueber J, Obrist D. Mercury in the Arctic tundra snowpack: temporal and spatial concentration patterns and trace gas exchanges. The Cryosphere 2018; 12: 1939-1956.

Ariya PA, Dastoor AP, Amyot M, Schroeder WH, Barrie L, Anlauf K, et al. The Arctic: a sink for mercury. Tellus Series B-Chemical and Physical Meteorology 2004; 56: 397-403.

Asner GP, Scurlock JMO, A. Hicke J. Global synthesis of leaf area index observations: implications for ecological and remote sensing studies: Global leaf area index. Global Ecology and Biogeography 2003; 12: 191-205.

Bargagli R, Agnorelli C, Borghini F, Monaci F. Enhanced deposition and bioaccumulation of mercury in Antarctic terrestrial ecosystems facing a coastal polynya. Environmental Science & Technology 2005; 39: 8150-8155.

Bari A, Rosso A, Minciardi MR, Troiani F, Piervittori R. Analysis of Heavy Metals in Atmospheric Particulates in Relation to Their Bioaccumulation in Explanted

Pseudevernia furfuracea Thalli. Environmental Monitoring and Assessment 2001; 69: 205-220.

Berg T, Steinnes E. Use of mosses (Hylocomium splendens and Pleurozium schreberi) as biomonitors of heavy metal deposition: From relative to absolute deposition values. Environmental Pollution 1997; 98: 61-71.

Bergquist BA, Blum JD. Mass-Dependent and -Independent Fractionation of Hg Isotopes by Photoreduction in Aquatic Systems. Science 2007; 318: 417-420.

Bergquist BA, Blum JD. The Odds and Evens of Mercury Isotopes: Applications of Mass-Dependent and Mass-Independent Isotope Fractionation. Elements 2009; 5: 353-357.

Bjorkman AD, Myers-Smith IH, Elmendorf SC, Normand S, Rüger N, Beck PSA, et al. Plant functional trait change across a warming tundra biome. Nature 2018.

Blum JD, Sherman LS, Johnson MW. Mercury Isotopes in Earth and Environmental Sciences. Annual Review of Earth and Planetary Sciences 2014; 42: 249-269.

Blum JD, Sherman LS, Keeler GJ, Douglas TA, Johnson KP, Barres JA. Mass-independent fractionation of mercury isotopes in Arctic snow driven by sunlight. Nature Geoscience 2010; 3: 173-177.

Brumbaugh WG, Morman SA, May TW. Concentrations and bioaccessibility of metals in vegetation and dust near a mining haul road, Cape Krusenstern National Monument, Alaska. Environmental Monitoring and Assessment 2011; 182: 325-340.

Buch AC, Correia MEF, Teixeira DC, Silva-Filho EV. Characterization of soil fauna under the influence of mercury atmospheric deposition in Atlantic Forest, Rio de Janeiro, Brazil. Journal of environmental sciences (China) 2015; 32: 217-227.

Campioli M, Samson R, Michelsen A, Jonasson S, Baxter R, Lemeur R. Nonvascular Contribution to Ecosystem Npp in a Subarctic Heath during Early and Late Growing Season. Plant Ecology 2009; 202: 41-53.

Carignan J, Estrade N, Sonke JE, Donard OFX. Odd isotope deficits in atmospheric Hg measured in lichens. Environmental science & technology 2009; 43: 5660.

Carignan J, Sonke J. The effect of atmospheric mercury depletion events on the net deposition flux around Hudson Bay, Canada. Atmospheric Environment 2010; 44: 4372-4379.

Carling GT, Rupper SB, Fernandez DP, Tingey DG, Harrison CB. Effect of Atmospheric Deposition and Weathering on Trace Element Concentrations in Glacial Meltwater at Grand Teton National Park, Wyoming, U.S.A. Arctic, Antarctic, and Alpine Research 2017; 49: 427-440.

Chapin FS, Shaver GR. Physiological and Growth Responses of Arctic Plants to a Field Experiment Simulating Climatic Change. Ecology 1996; 77: 822-840.

Chow JC, Watson JG, Houck JE, Pritchett LC, Fred Rogers C, Frazier CA, et al. A laboratory resuspension chamber to measure fugitive dust size distributions and chemical compositions. Atmospheric Environment 1994; 28: 3463-3481.

Dastoor A, Ryzhkov A, Durnford D, Lehnherr I, Steffen A, Morrison H. Atmospheric mercury in the Canadian Arctic. Part II: Insight from modeling. Science of the Total Environment 2015; 509-510: 16-27.

Dastoor AP, Durnford DA. Arctic Ocean: Is It a Sink or a Source of Atmospheric Mercury? Environmental Science & Technology 2014; 48: 1707-1717.

Dastoor AP, Larocque Y. Global circulation of atmospheric mercury: a modelling study. Atmospheric Environment 2004; 38: 147-161.

Demers JD, Blum JD, Zak DR. Mercury isotopes in a forested ecosystem: Implications for air-surface exchange dynamics and the global mercury cycle. Global Biogeochemical Cycles 2013; 27: 222-238.

Derry LA, Chadwick OA. Contributions from Earth's Atmosphere to Soil. Elements 2007; 3: 333-338.

Douglas TA, Loseto LL, Macdonald RW, Outridge P, Dommergue A, Poulain A, et al. The fate of mercury in Arctic terrestrial and aquatic ecosystems, a review. Environmental Chemistry 2012; 9: 321.

Douglas TA, Sturm M. Arctic haze, mercury and the chemical composition of snow across northwestern Alaska. Atmospheric Environment 2004; 38: 805-820.

Drbal K, Elster J, Komarek J. Heavy metals in water, ice and biological material from Spitsbergen, Svalbard. Polar research 1992; 11: 99-101.

Dunec JL. The fate, transport, and ecological impacts of airborne contaminants in western national parks. 23. American Bar Association, Chicago, 2008, pp. 54.

Durnford D, Dastoor A, Figueras-Nieto D, Ryjkov A. Long range transport of mercury to the Arctic and across Canada. Atmospheric Chemistry and Physics 2010; 10: 6063-6086.

Enrico M, Roux GL, Heimbürger L-E, Beek PV, Souhaut M, Chmeleff J, et al. Holocene Atmospheric Mercury Levels Reconstructed from Peat Bog Mercury Stable Isotopes. Environmental Science & Technology 2017; 51: 5899.

Enrico M, Roux GL, Marusczak N, Heimbürger L-E, Claustres A, Fu X, et al. Atmospheric Mercury Transfer to Peat Bogs Dominated by Gaseous Elemental Mercury Dry Deposition. Environmental science & technology 2016; 50: 2405.

EPA U. Method 1631, revision E: mercury in water by oxidation, purge and trap, and cold vapor atomic fluorescence spectrometry, US Environmental Protection Agency, Washington DC, 2002.

EPA U. Method 7473, Mercury in Solids and Solutions by Thermal Decomposition, Amalgamation, and Atomic Absorption Spectrometry. U.S. Government Printing Office, Washington D.C., 2000.

Ericksen J, Gustin M. Foliar exchange of mercury as a function of soil and air mercury concentrations. Science of the Total Environment 2004a; 324: 271-279.

Ericksen JA, Gustin MS, Schorran DE, Johnson DW, Lindberg SE, Coleman JS. Accumulation of atmospheric mercury in forest foliage. Atmospheric Environment 2003; 37: 1613-1622.

Estrade N, Carignan J, Donard OFX. Isotope Tracing of Atmospheric Mercury Sources in an Urban Area of Northeastern France. Environmental Science & Technology 2010; 44: 6062-6067.

Ferrari CP, Gauchard P-A, Aspmo K, Dommergue A, Magand O, Bahlmann E, et al. Snow-to-air exchanges of mercury in an Arctic seasonal snow pack in Ny-Ålesund, Svalbard. Atmospheric Environment 2005; 39: 7633-7645.

Frescholtz TF, Gustin MS, Schorran DE, Fernandez GCJ. Assessing the source of mercury in foliar tissue of quaking aspen. Environmental Toxicology and Chemistry 2003; 22: 2114-2119.

Grigal DF. Mercury sequestration in forests and peatlands: A review. Journal of Environmental Quality 2003; 32: 393-405.

Grigal DF, Kolka RK, Fleck JA, Nater EA. Mercury Budget of an Upland-Peatland Watershed. Biogeochemistry 2000; 50: 95-109.

Hall BD, St Louis VL. Methylmercury and total mercury in plant litter decomposing in upland forests and flooded landscapes. Environmental science & technology 2004; 38: 5010-5021.

Hanson PJ, Lindberg S, Tabberer T, Owens J, Kim K-H. Foliar exchange of mercury vapor: evidence for a compensation point. Water Air and Soil Pollution 1995; 80: 373-382.

Hojdová M, Rohovec J, Chrastný V, Penížek V, Navrátil T. The Influence of Sample Drying Procedures on Mercury Concentrations Analyzed in Soils. Bulletin of Environmental Contamination and Toxicology. 2015; 94: 570-576.

Holt EA, Bench G. 14C/C measurements support Andreev's internode method to determine lichen growth rates in Cladonia stygia (Fr.) Ruoss. The Lichenologist 2008; 40: 559-565.

Ikingura JR, Akagi H. Lichens as a Good Bioindicator of Air Pollution by Mercury in Small-Scale Gold Mining Areas, Tanzania. Bulletin of Environmental Contamination and Toxicology 2002; 68: 699-704.

Jaeglé L. Atmospheric long-range transport and deposition of mercury to Alaska. Department of Atmospheric Sciences, University of Washington, Seattle, A report to the Alaska Department of Environmental Conservation, 2010.

Jiskra M, Sonke JE, Obrist D, Bieser J, Ebinghaus R, Myhre CL, et al. A vegetation control on seasonal variations in global atmospheric mercury concentrations. Nature Geoscience 2018; 11: 244-250.

Jiskra M, Wiederhold JG, Skyllberg U, Kronberg RM, Hajdas I, Kretzschmar R. Mercury Deposition and Re-emission Pathways in Boreal Forest Soils Investigated with Hg Isotope Signatures. Environmental Science & Technology 2015; 49: 7188-7196.

Johnson KP, Blum JD, Keeler GJ, Douglas TA. Investigation of the deposition and emission of mercury in arctic snow during an atmospheric mercury depletion event. Journal of Geophysical Research - Atmospheres 2008; 113: D17304.

Kolka RK, Nater EA, Grigal DF, Verry ES. Atmospheric inputs of mercury and organic carbon into a forested upland bog watershed. Water Air and Soil Pollution 1999; 113: 273-294.

Koster van Groos PG, Esser BK, Williams RW, Hunt JR. Isotope effect of mercury diffusion in air. Environmental science & technology 2014; 48: 227-233.

Kritee K, Blum JD, Johnson MW, Bergquist BA, Barkay T. Mercury stable isotope fractionation during reduction of Hg(II) to Hg(0) by mercury resistant microorganisms. Environmental science & technology. 2007; 41: 1889-1895.

Laacouri A, Nater EA, Kolka RK. Distribution and Uptake Dynamics of Mercury in Leaves of Common Deciduous Tree Species in Minnesota, USA. Environmental science & technology 2013; 47: 10462-10470.

Landers DH, Ford J, Gubala C, Monetti M, Lasorsa BK, Martinson J. Mercury in vegetation and lake sediments from the U. S. arctic. Water, Air, & Soil Pollution 1995; 80: 591-601.

Lindberg SE. Forests and the Global Biogeochemical Cycle of Mercury: The Importance of Understanding Air/Vegetation Exchange Processes. In: Baeyens W, Ebinghaus R, Vasiliev O, editors. Global and Regional Mercury Cycles: Sources, Fluxes and Mass Balances. 21. Springer Netherlands, 1996, pp. 359-380.

Lindberg SE, Brooks S, Lin CJ, Scott KJ, Landis MS, Stevens RK, et al. Dynamic oxidation of gaseous mercury in the Arctic troposphere at polar sunrise. Environmental Science & Technology 2002; 36: 1245-1256.

McTainsh G, Strong C. The role of aeolian dust in ecosystems. Geomorphology 2007; 89: 39-54.

Millhollen A, Obrist D, Gustin M. Mercury accumulation in grass and forb species as a function of atmospheric carbon dioxide concentrations and mercury exposures in air and soil. Chemosphere 2006b; 65: 889-897.

Moore CW, Obrist D*, Steffen A, Staebler RM, Douglas TA, Richter A, Nghiem SV. Convective forcing of mercury and ozone in the Arctic boundary layer by lead in sea ice. Nature, doi:10.1038/nature12924, 2014. (*Equal Contributions).

Muller SV, Racoviteanu AE, Walker DA. Landsat MSS-derived land-cover map of northern Alaska: Extrapolation methods and a comparison with photo-interpreted and AVHRR-derived maps. International Journal of Remote Sensing 1999; 20: 2921-2946.

Munthe J, Hultberg H, Iverfeldt A. Mechanisms of deposition of methylmercury and mercury to coniferous forests. Water Air and Soil Pollution 1995; 80: 363-371.

Nakano T, Yokoo Y, Okumura M, Jean S-R, Satake K. Evaluation of the Impacts of Marine Salts and Asian Dust on the Forested Yakushima Island Ecosystem, a World Natural Heritage Site in Japan. Water, Air, & Soil Pollution 2012; 223: 5575-5597.

Narasimhan R, Stow D. Daily MODIS products for analyzing early season vegetation dynamics across the North Slope of Alaska. Remote Sensing of Environment 2010; 114: 1251-1262.

Nickel S, Hertel A, Pesch R, Schröder W, Steinnes E, Uggerud HT. Correlating concentrations of heavy metals in atmospheric deposition with respective accumulation in moss and

natural surface soil for ecological land classes in Norway between 1990 and 2010. Environmental Science and Pollution Research 2015; 22: 8488-8498.

Nowak DJ, Crane DE, Stevens JC. Air pollution removal by urban trees and shrubs in the United States. Urban Forestry & Urban Greening 2006; 4: 115-123.

Obrist D, Agnan Y, Jiskra M, Olson CL, Colegrove DP, Hueber J, et al. Tundra uptake of atmospheric elemental mercury drives Arctic mercury pollution. Nature 2017; 547: 201.

Obrist D, Pearson C, Webster J, Kane T, Lin C-J, Aiken GR, et al. A synthesis of terrestrial mercury in the western United States: Spatial distribution defined by land cover and plant productivity. Science of The Total Environment 2016; 568: 522-535.

Obrist D. Mercury distribution across 14 U.S. forests. Part II: Patterns of methyl mercury concentrations and areal mass of total and methyl mercury. Environmental science & technology. 2012; 46: 5921-5930.

Obrist D, Johnson DW, Lindberg SE, Luo Y, Hararuk O, Bracho R, et al. Mercury distribution across 14 U.S. Forests. Part I: spatial patterns of concentrations in biomass, litter, and soils. Environ Sci Technol 2011; 45: 3974-81.

Obrist D, Hallar AG, McCubbin I, Stephens BB, Rahn T. Atmospheric mercury concentrations at Storm Peak Laboratory in the Rocky Mountains: Evidence for long-range transport from Asia, boundary layer contributions, and plant mercury uptake. Atmospheric Environment 2008; 42: 7579-7589.

Obrist D. Atmospheric Mercury Pollution Due to Losses of Terrestrial Carbon Pools? Biogeochemistry 2007; 85: 119-123.

Olson C, Jiskra M, Biester H, Chow J, Obrist D. Mercury in Active-Layer Tundra Soils of Alaska: Concentrations, Pools, Origins, and Spatial Distribution. Global Biogeochemical Cycles 2018.

Park T, Ganguly S, Tømmervik H, Euskirchen ES, Høgda K-A, Karlsen SR, et al. Changes in growing season duration and productivity of northern vegetation inferred from long-term remote sensing data. Environmental Research Letters 2016; 11: 84001.

Pearson RG, Phillips SJ, Loranty MM, Beck PSA, Damoulas T, Knight SJ, et al. Shifts in Arctic vegetation and associated feedbacks under climate change. Nature Climate Change 2013; 3: 673-677.

Ram SS, Majumder S, Chaudhuri P, Chanda S, Santra SC, Maiti PK, et al. Plant canopies: bio-monitor and trap for re-suspended dust particulates contaminated with heavy metals. Mitigation and Adaptation Strategies for Global Change 2014; 19: 499-508.

Rasmussen PE. Temporal variation of mercury in vegetation. Water, Air, & Soil Pollution 1995; 80: 1039-1042.

Rasmussen PE, Mierle G, Nriagu JO. The analysis of vegetation for total mercury. Water, Air, & Soil Pollution 1991; 56: 379-390.

Rea AW, Keeler GJ, Scherbatskoy T. The deposition of mercury in throughfall and litterfall in the lake champlain watershed: A short-term study. Atmospheric Environment 1996; 30: 3257-3263.

Rea AW, Lindberg SE, Scherbatskoy T, Keeler GJ. Mercury Accumulation in Foliage over Time in Two Northern Mixed-Hardwood Forests. Water, Air, and Soil Pollution 2002; 133: 49-67.

Reimann C, Englmaier P, Flem B, Gough L, Lamothe P, Nordgulen Ø, et al. Geochemical gradients in soil O-horizon samples from southern Norway: Natural or anthropogenic? Applied Geochemistry 2009; 24: 62-76.

Riget F, Asmund G, Aastrup P. Mercury in Arctic char (Salvelinus alpinus) populations from Greenland. Science of the Total Environment 2000; 245: 161-172.

Riis T, Christoffersen KS, Baattrup-Pedersen A. Effects of warming on annual production and nutrient-use efficiency of aquatic mosses in a high Arctic lake. Freshwater Biology 2014; 59: 1622-1632.

Risch MR, Dewild JF, Krabbenhoft DP, Kolka RK, Zhang L. Litterfall mercury dry deposition in the eastern USA. Environ Pollut 2012; 161: 284-90.

Risch MR, Kenski DM. Spatial Patterns and Temporal Changes in Atmospheric-Mercury Deposition for the Midwestern USA, 2001-2016. Atmosphere 2018; 9: 29.

Rutter AP, Schauer JJ, Shafer MM, Creswell JE, Olson MR, Robinson M, et al. Dry deposition of gaseous elemental mercury to plants and soils using mercury stable isotopes in a controlled environment. Atmospheric Environment 2011; 45: 848-855.

Rühling Å, Rasmussen L, Pilegaard K, Maekinen A, Steinnes E. Survey of atmospheric heavy metal deposition in the Nordic countries in 1985 monitored by moss analyses. NMR, 1987.

Santelmann MV, Gorham E. The Influence of Airborne Road Dust on the Chemistry of Sphagnum Mosses. Journal of Ecology 1988; 76: 1219-1231.

Santolaria Z, Arruebo T, Pardo A, Rodríguez-Casals C, Matesanz JM, Lanaja FJ, et al. Natural and anthropic effects on hydrochemistry and major and trace elements in the water mass

of a Spanish Pyrenean glacial lake set. Environmental Monitoring and Assessment 2017; 189: 1-16.

Schulze ED. Plant Life Forms and Their Carbon, Water and Nutrient Relations. In: Lange OL, Nobel PS, Osmond CB, Ziegler H, editors. Physiological Plant Ecology II: Water Relations and Carbon Assimilation. Springer Berlin Heidelberg, Berlin, Heidelberg, 1982, pp. 615-676.

Schuster PF, Schaefer KM, Aiken GR, et al. Permafrost Stores a Globally Significant Amount of Mercury. Geophysical Research Letters. 2018; 45: 1463-1471.

Schwesig D, Matzner E. Dynamics of mercury and methylmercury in forest floor and runoff of a forested watershed in Central Europe. Biogeochemistry 2001; 53: 181-200.

Shahid M, Dumat C, Khalid S, Schreck E, Xiong T, Niazi NK. Foliar heavy metal uptake, toxicity and detoxification in plants: A comparison of foliar and root metal uptake. Journal of Hazardous Materials 2017; 325: 36-58.

Shaver GR, Chapin FS. Production - Biomass Relationships and Element Cycling in Contrasting Arctic Vegetation Types. Ecological Monographs 1991; 61: 1-31.

Shotyk W, Bicalho B, Cuss CW, Duke MJM, Noernberg T, Pelletier R, et al. Dust is the dominant source of "heavy metals" to peat moss (Sphagnum fuscum) in the bogs of the Athabasca Bituminous Sands region of northern Alberta. 2016; 92-93: 494.

Simonich SL, Hites RA. Importance of vegetation in removing polycyclic aromatic-hydrocarbons from the atmosphere. Nature 1994; 370: 49-51.

Skov H, Christensen JH, Goodsite ME, Heidam NZ, Jensen B, Wahlin P, et al. Fate of elemental mercury in the arctic during atmospheric mercury depletion episodes and the load of

atmospheric mercury to the arctic. Environmental Science & Technology 2004; 38: 2373-2382.

Sloof JE. Lichens as quantitative biomonitors for atmospheric trace-element deposition, using transplants. Atmospheric Environment 1995; 29: 11-20.

Smith RS, Wiederhold JG, Jew AD, Brown JGE, Bourdon B, Kretzschmar R. Stable Hg isotope signatures in creek sediments impacted by a former Hg mine. Environmental science & technology 2015; 49: 767-776.

Sonke JE. A global model of mass independent mercury stable isotope fractionation. Geochimica et Cosmochimica Acta 2011; 75: 4577-4590.

St Pierre KA, St Louis VL, Kirk JL, Lehnherr I, Wang S, La Farge C. Importance of open marine waters to the enrichment of total mercury and monomethylmercury in lichens in the canadian high arctic. Environ Sci Technol 2015; 49: 5930-8.

Stamenkovic J, Gustin MS. Nonstomatal versus Stomatal Uptake of Atmospheric Mercury. Environmental science & technology 2009; 43: 1367-1372.

Stamenkovic J, Gustin MS, Arnone JA, Johnson DW, Larsen JD, Verburg PSJ. Atmospheric mercury exchange with a tallgrass prairie ecosystem housed in mesocosms. Science of the Total Environment 2008; 406: 227-238.

Steffen A, Douglas T, Amyot M, Ariya P, Aspmo K, Berg T, et al. A synthesis of atmospheric mercury depletion event chemistry in the atmosphere and snow. Atmospheric Chemistry and Physics 2008; 8: 1445-1482.

Steffen A, Lehnherr I, Cole A, Ariya P, Dastoor A, Durnford D, et al. Atmospheric mercury in the Canadian Arctic. Part I: A review of recent field measurements. Science of the Total Environment 2015; 509: 3-15.

Steinnes E. A critical evaluation of the use of naturally growing moss to monitor the deposition of atmospheric metals. Science of the Total Environment 1995; 160: 243-249.

Steinnes E, Berg T, Sjobakk TE. Temporal and spatial trends in Hg deposition monitored by moss analysis. Science of the Total Environment 2003; 304: 215-219.

Steinnes E, Sjobakk TE. Order-of-magnitude increase of Hg in Norwegian peat profiles since the outset of industrial activity in Europe. Environmental Pollution 2005; 137: 365-370.

Sun LM, Lu BY, Yuan DX, Hao WB, Zheng Y. Variations in the isotopic composition of stable mercury isotopes in typical mangrove plants of the Jiulong estuary, SE China. Environmental Science and Pollution Research 2017; 24: 1459-1468.

Sun R, Enrico M, Heimbürger L-E, Scott C, Sonke JE. A double-stage tube furnace—acid-trapping protocol for the pre-concentration of mercury from solid samples for isotopic analysis. Analytical and Bioanalytical Chemistry 2013; 405: 6771-6781.

Tape KEN, Sturm M, Racine C. The evidence for shrub expansion in Northern Alaska and the Pan-Arctic. Global Change Biology 2006; 12: 686-702.

U.S. EPA (1999). Method IO 3.3, Compendium of Methods for the Determination of Inorganic Compounds in Ambient Air. Washington, DC.

Van Dam B, Helmig D, Doskey PV, Oltmans SJ. Summertime surface O3 behavior and deposition to tundra in the Alaskan Arctic. Journal of Geophysical Research: Atmospheres 2016; 121: 8055-8066.

Wang X, Bao ZD, Lin CJ, Yuan W, Feng XB. Assessment of Global Mercury Deposition through Litterfall. Environmental science & technology 2016; 50: 8548-8557.

Wang X, Luo J, Yin R, Yuan W, Lin C-J, Sommar J, et al. Using Mercury Isotopes To Understand Mercury Accumulation in the Montane Forest Floor of the Eastern Tibetan Plateau. Environmental Science & Technology 2017; 51: 801.

Willkomm H, Bölter M, Kappen L. 14C activity of Antarctic lichens. PANGAEA, 1992.

Wojtun B, Samecka-Cymerman A, Kolon K, Kempers AJ, Skrzypek G. Metals in some dominant vascular plants, mosses, lichens, algae, and the biological soil crust in various types of terrestrial tundra, SW Spitsbergen, Norway. Polar Biology 2013; 36: 1799-1809.

Yang Y, Yanai RD, Montesdeoca M, Driscoll CT. Measuring mercury in wood: challenging but important. International journal of environmental analytical chemistry 2017; 97: 456-67.

Yin R, Feng X, Hurley JP, Krabbenhoft DP, Lepak RF, Hu R, et al. Mercury Isotopes as Proxies to Identify Sources and Environmental Impacts of Mercury in Sphalerites. Scientific reports 2016; 6: 18686.

Yin R, Feng X, Li X, Yu B, Du B. Trends and advances in mercury stable isotopes as a geochemical tracer. Trends in Environmental Analytical Chemistry 2014; 2: 1-10.

Yin R, Feng X, Meng B. Stable mercury isotope variation in rice plants (Oryza sativa L.) from the Wanshan mercury mining district, SW China. Environmental science & technology 2013; 47: 2238.

Yuan W, Sommar J, Lin CJ, Wang X, Li K, Liu Y, Zhang H, Lu Z, Wu C, Feng X. Stable isotope evidence shows re-emission of elemental mercury vapor occurring after reductive loss from foliage. Environmental Science & Technology 2018. DOI: 10.1021/acs.est.8b04865

Zheng W, Hintelmann H. Mercury isotope fractionation during photoreduction in natural water is controlled by its Hg/DOC ratio. Geochimica et Cosmochimica Acta 2009; 73: 6704-6715.

Zheng W, Hintelmann H. Isotope fractionation of mercury during its photochemical reduction by low-molecular-weight organic compounds. The journal of physical chemistry. 2010a; 114: 4246.

Zheng W, Hintelmann H. Nuclear Field Shift Effect in Isotope Fractionation of Mercury during Abiotic Reduction in the Absence of Light. Journal of Physical Chemistry A 2010b; 114: 4238-4245.

Zheng W, Obrist D, Weis D, Bergquist BA. Mercury isotope compositions across North American forests. Global Biogeochemical Cycles 2016; 30: 1475-1492.

Figure 1. Research sites used in this study. a. The main research site was a Tussock tundra located at Toolik Field Station in northern Alaska. Another site was located at Eight Mile Lake Observatory near Denali National Park in interior Alaska. In addition, seven sites (b.) were chosen along a 200 km transect following the Dalton Highway from Toolik Field Station north to Deadhorse, AK near the Arctic Coast.

Figure 2. Mean mercury (Hg) concentrations (in µg kg^{-1}) in bulk vegetation and different species and functional groups across all Alaskan sites including Betula Nana leaves (dwarf birch), Carex aquatic (tussock grass), Sphagnum (peat moss), Masonhalea richardsonnii (brown lichen), Bulk Vegetation, and Hylocomium splendens (feather moss). Uncertainty is expressed by the standard error bars.

Figure 3. Density plots, medians, and ranges of mercury (Hg) concentrations in Alaskan Arctic vegetation separated for various functional vegetation types, including grasses, herbaceous leaves, moss, and lichen. Data include vegetation samples collected in this study and from six published studies (n=150) (Drbal et al., 1992; Landers et al., 1995; Riget et al., 2000; St Pierre et al., 2015; Steinnes et al., 2003; Wojtun et al., 2013).

Figure 4. Mean mercury (Hg) concentrations (µg kg^{-1}) in tussock grass (*Carex Aquatis*) (top panel) and in bulk vegetation (bottom panel) from vegetation samples collected across all study sites in central and northern Alaska. EMLO stands for Eight Mile Lake Observatory near Denali National Park. Uncertainty is expressed by the standard error bars.

Figure 5. Increases in Hg vegetation concentrations at the Toolik Field station during the summers of 2015 and 2016. Early season sampling of vegetation was performed in June and July. Late season sampling was performed in August and September. Uncertainty is expressed by the standard error bars.

Figure 6. Mass-dependent ($\delta^{202}Hg$) vs. odd mass-independent ($\Delta^{199}Hg$) (left) and mass-dependent ($\delta^{202}Hg$) vs. even mass-independent ($\Delta^{200}Hg$) (right) mercury isotope signatures in different species of tundra vegetation collected at Toolik Field Station, including *Carex aquatic* (tussock grass), *Betula Nana* (dwarf birch) leaves, *Masonhalea richardsonnii* (brown lichen), *Cetraria islandica* (white lichen) *Hylocomium splendens* (feather moss), *Sphagnum* (peat moss), and bulk vegetation. Atmospheric Hg(0) (grey squares) and wet deposition (blue triangles) isotope measurements from the Toolik Field station were also included. Values from atmospheric Hg(0), wet deposition and bulk vegetation are from Obrist et al. (2017). The error bars shown in the lower left corner represent two times the standard deviation of replicate measurements of the in-house standard (ETH-Fluka).

Highlights

- Arctic vegetation plays a critical role in the uptake and cycling of Hg into tundra ecosystems
- Aboveground biomass Hg pools (29 μg m^{-2}) were in a similar range of those measured at temperature sites, despite the remoteness and short growing season of the Arctic
- High bulk vegetation Hg concentrations and pool sizes were attributed to the significant contribution of nonvascular plants with high Hg concentrations
- Stable Hg isotope analysis confirmed dominant Hg(0) source to tundra vegetation with little evidence of photochemical Hg(II) reduction and revolatilization

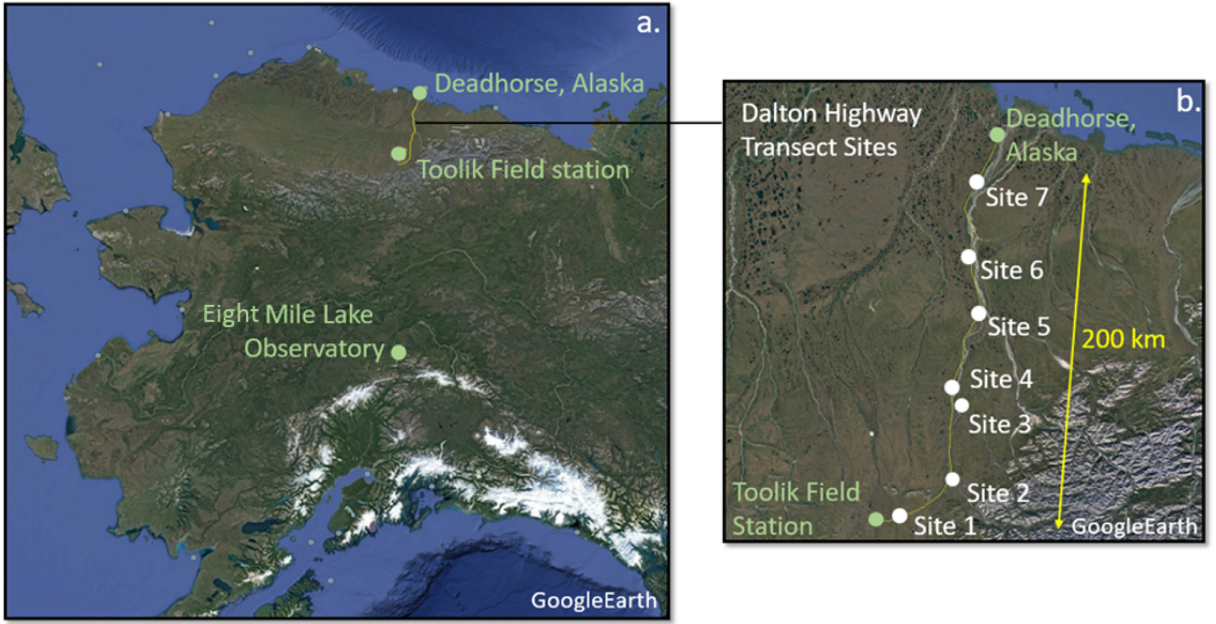
a.
Deadhorse, Alaska
Toolik Field station
Eight Mile Lake
Observatory
GoogleEarth
b.
Dalton Highway
Transect Sites
Deadhorse,
Alaska
Site 7
Site 6
Site 5
200 km
Site 4
Site 3
Site 2
Toolik Field
Station
Site 1
GoogleEarth

Figure 1

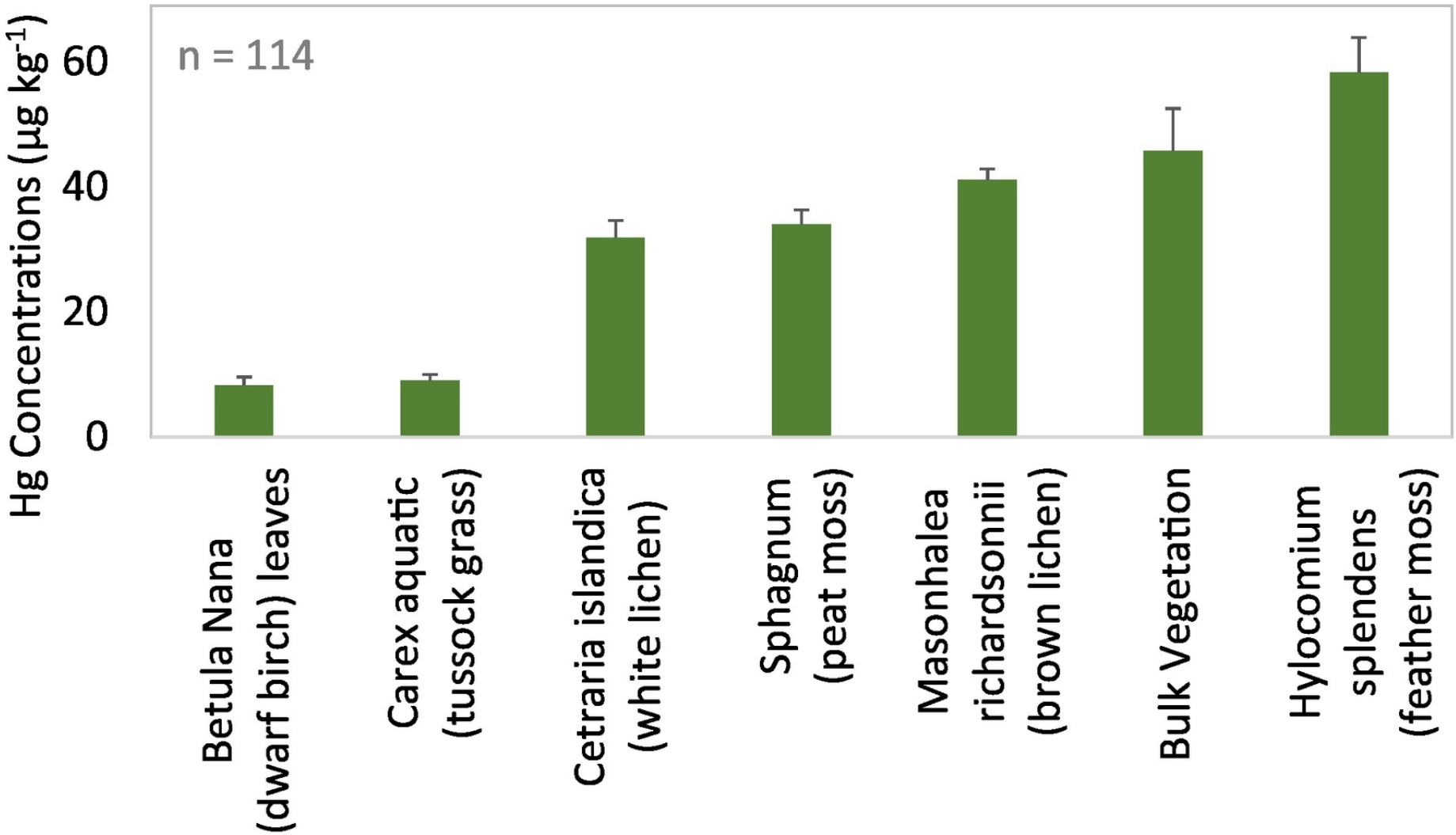
n = 114
Hg Concentrations (µg kg-1)
60
40
20
0
Betula Nana (dwarf birch) leaves
Carex aquatic (tussock grass)
Cetraria islandica (white lichen)
Sphagnum (peat moss)
Masonhalea richardsonnii (brown lichen)
Bulk Vegetation
Hylocomium splendens (feather moss)

Figure 2

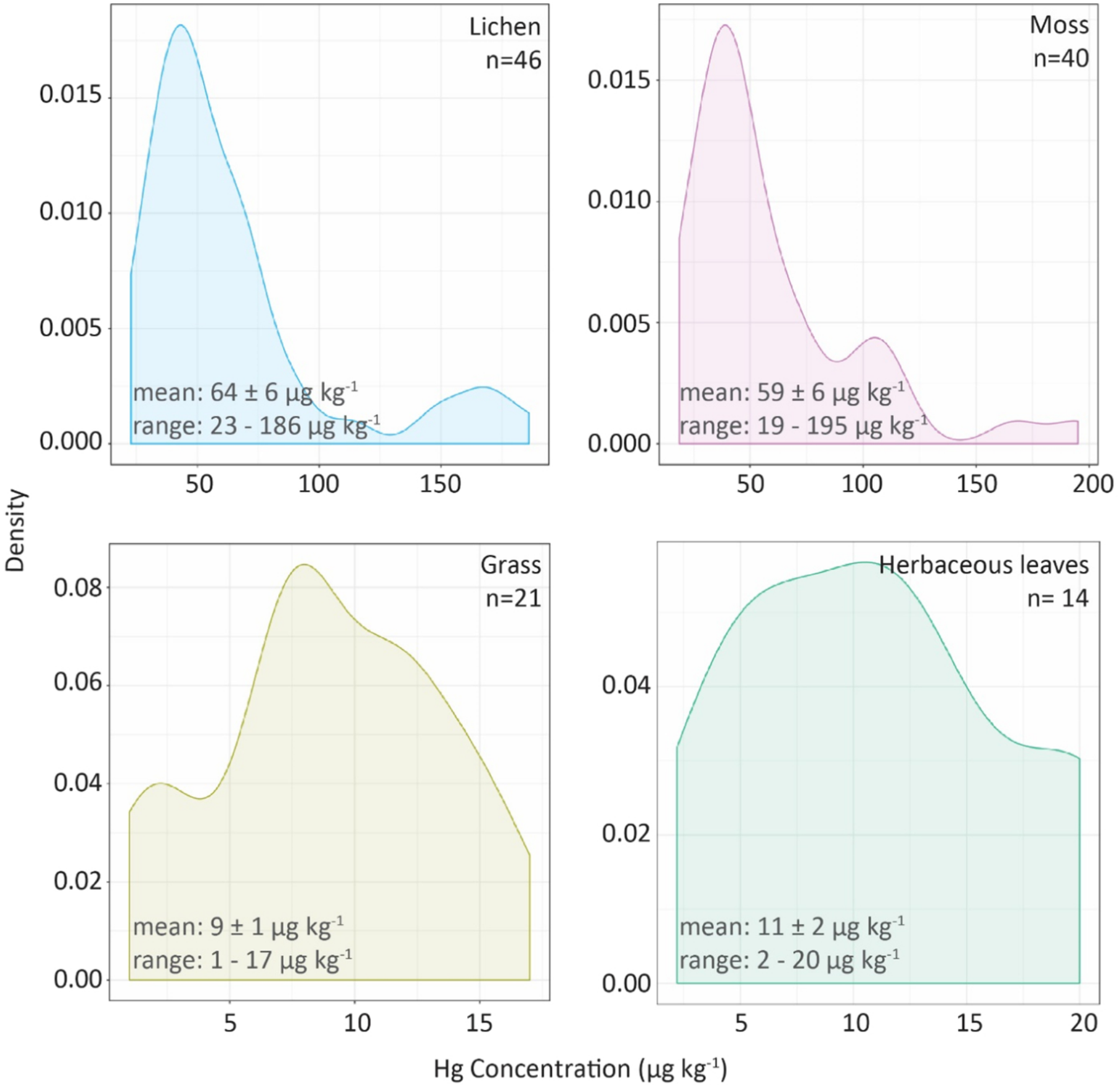
Lichen
n=46
mean: 64 ± 6 µg kg-1
range: 23 - 186 µg kg-1
Moss
n=40
mean: 59 ± 6 µg kg-1
range: 19 - 195 µg kg-1
Grass
n=21
mean: 9 ± 1 µg kg-1
range: 1 - 17 µg kg-1
Herbaceous leaves
n= 14
mean: 11 ± 2 µg kg-1
range: 2 - 20 µg kg-1
Density
Hg Concentration (µg kg-1)

Figure 3

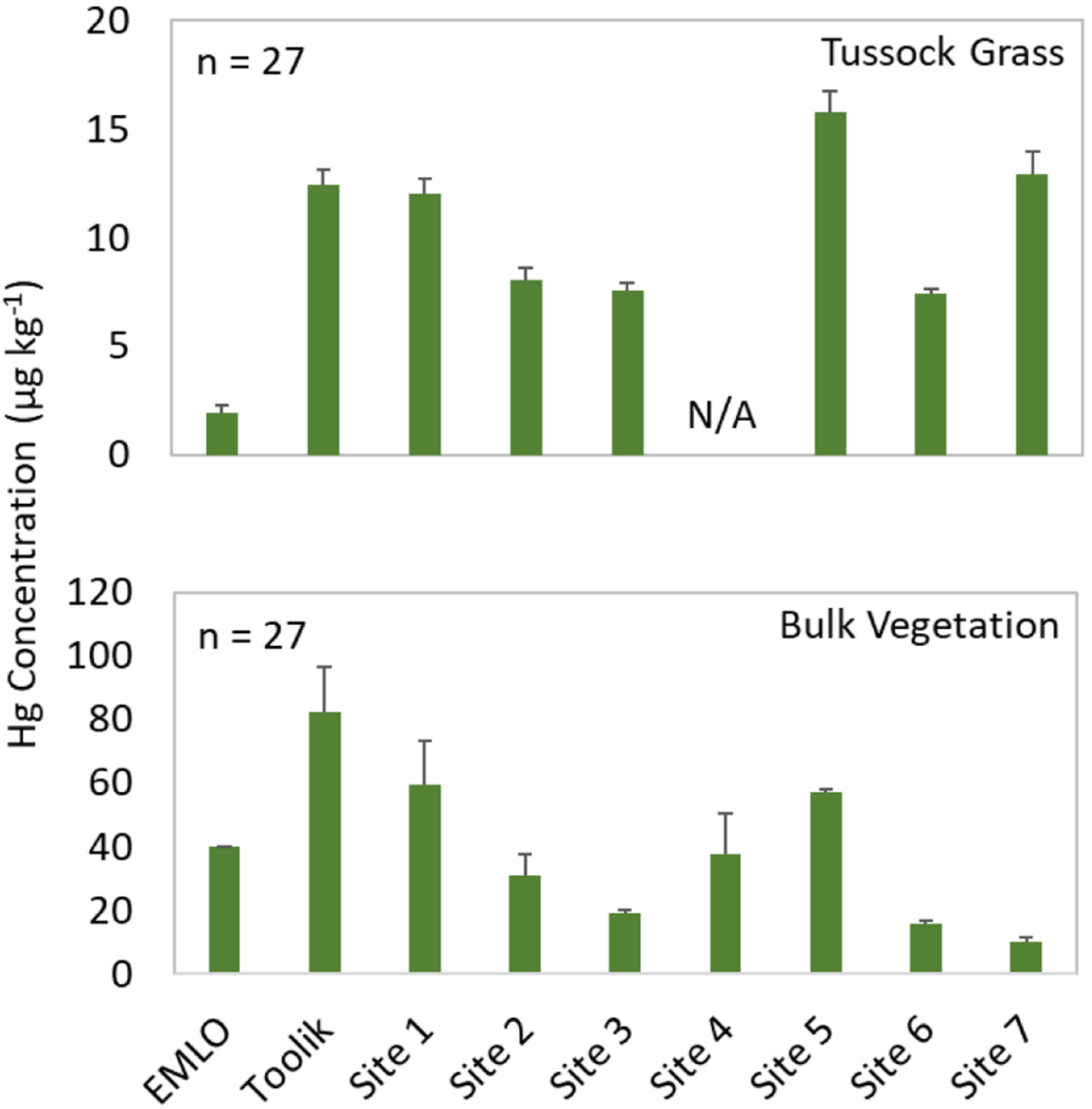
n = 27
Tussock Grass
20
15
10
5
0
N/A
n = 27
Bulk Vegetation
120
100
80
60
40
20
0
Hg Concentration (µg kg-1)
EMLO
Toolik
Site 1
Site 2
Site 3
Site 4
Site 5
Site 6
Site 7

Figure 4

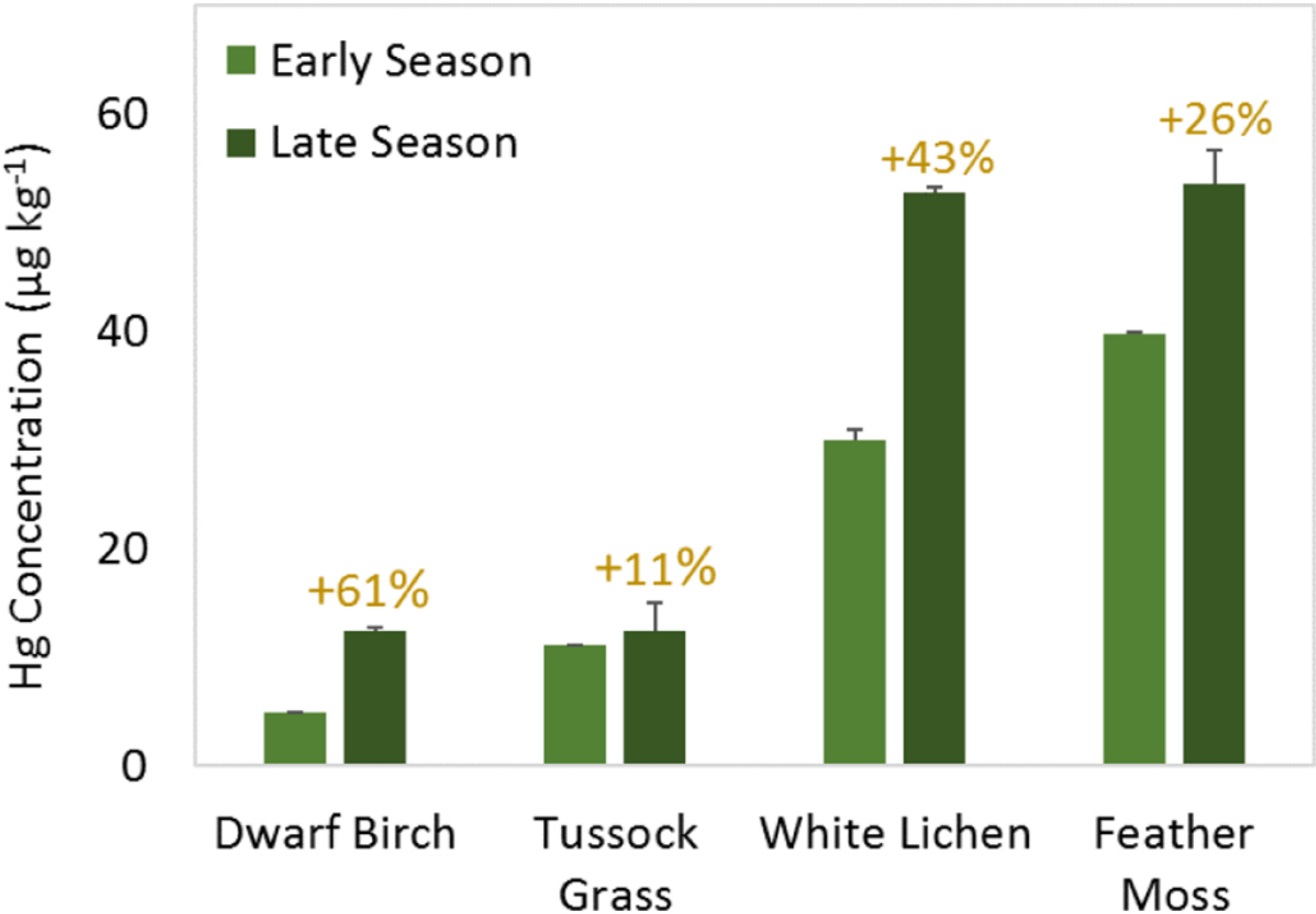
Early Season
Late Season
Hg Concentration (µg kg-1)
60
40
20
0
+61%
+11%
+43%
+26%
Dwarf Birch
Tussock Grass
White Lichen
Feather Moss

Figure 5

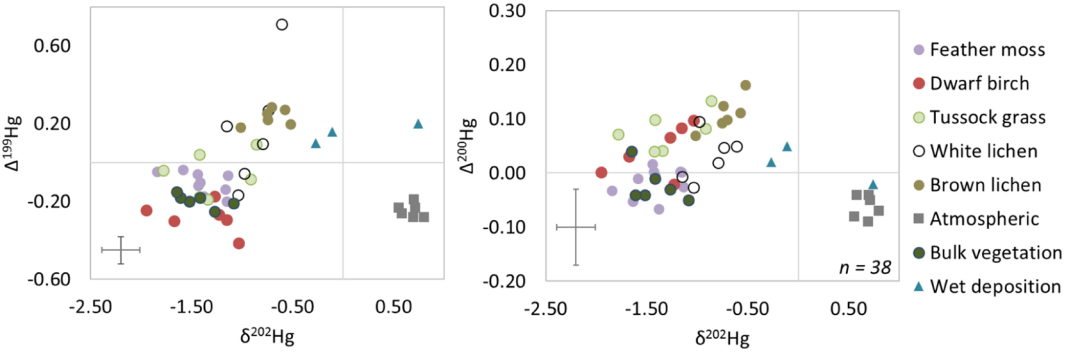
0.60
0.20
-0.20
-0.60
-2.50
-1.50
-0.50
0.50
δ202Hg
Δ199Hg
0.30
0.20
0.10
0.00
-0.10
-0.20
-2.50
-1.50
-0.50
0.50
δ202Hg
Δ200Hg
n = 38
Feather moss
Dwarf birch
Tussock grass
White lichen
Brown lichen
Atmospheric
Bulk vegetation
Wet deposition

Figure 6